scientific reports



OPEN Water footprint management in textile industry through Acid Blue 113 remediation using halloysite nanoclay as a sustainable adsorbent

Mohammed A. H. Dhaif Allah¹, Syed Noeman Tagui², Usman Tagui Syed³, Syida Aameera Yakuth⁴, Razia Sulthana⁴, Rayees Afzal Mir⁵, Akheel Ahmed Syed^{6⊠}, Shareefraza J. Ukkund⁷, Majed Alsubih⁸, Saiful Islam⁸ & Wahaj Ahmad Khan^{9⊠}

Experimental studies were carried out to adsorb Acid Blue 113 (AB113), an azo dye that is probably a mutagen, from aqueous environments using commercially available, inexpensive halloysite nanoclay (HNC). Water footprint management in the remediation of dye from aqueous medium and textile industrial effluent (TIE) was the focus of a laboratory-scale experiment planned and carried out to align with the guidelines of sustainability and valorization. One interesting feature of this study is that the adsorption process is almost independent of the temperature (27-50 °C) and pH (2-12) range studied, which aligns with sustainability and valorization necessities. We conducted a laboratoryscale experiment to assess the water footprint of textile industrial effluent (TIE). To determine how operational factors affected the effectiveness of dye removal, we looked into initial dye concentration $(25-200 \text{ mg L}^{-1})$, contact time (15-180 min), adsorbent dosage $(0.500-6.000 \text{ g L}^{-1})$, initial pH (2-12), and temperature (30-50 °C). The findings showed that higher initial dye concentration, a 60-min contact time, and a pH range of 2–12 provide dye removal efficiency ($q_a = 95.00 \text{ mg g}^{-1}$). A two-level fractional factorial experimental design (FFED) was employed to determine the factors influencing HNC's adsorption capacity and evaluate the feasibility and effectiveness of the approach. The optimal values of the variables were determined using interaction factors derived from multiple regression studies based on FFED to maximize the second-order polynomial equation. Under optimal conditions of pH 1, the adsorbent dosage of 0.500 g L⁻¹, beginning dye concentration of 623 mg L⁻¹, adsorption time of 139 min with orbital shaking of 165 rpm at 49 °C, the maximum adsorption value achieved by statistical optimization was 329 mg q⁻¹. Four two-parameter and six three-parameter isotherm models were used to analyze equilibrium data. The pseudo-first-order and pseudo-second-order models were applied in our adsorption kinetic investigations. Webber-Morris, Dumwald-Wagner, and film diffusion models were used to examine the diffusion effects. The adsorption system's thermodynamic parameters, Gibbs free energy (ΔG^0), entropy (ΔS^0), and change in enthalpy (ΔH^0) were also measured and assessed. Fourier transform infrared spectroscopy (FTIR) and scanning electron microscopy (SEM) were used to characterize the dye, the adsorbent, and the dye-adsorbed HNC. The experiments showed that HNC is an economical and efficient adsorbent for eliminating AB113 dye from aqueous solutions and effluent from the textile industry. It is possible to use the dye-adsorbed HNC, known as "sludge", as a strengthening material for creating composites from waste plastic. Preliminary research examined and contrasted the physico-mechanical and chemical characteristics of dye-adsorbed HNC thermoplastic and thermoset composites with those of HNC composites.

Keywords Halloysite nanoclay, Acid Blue 113, Modelling, Water footprint, Textile industrial effluent

¹Department of Agriculture, Faculty of Agriculture and Veterinary Medicine, Thamar University, Dhamar, Republic of Yemen. ²Department of Studies in Chemistry, Bharathi College - Post Graduate and Research Centre, Bharathi Nagara, Karnataka 571422, India. ³LAQV-REQUIMTE, Department of Chemistry, Faculty of Science and Technology, Universidade NOVA de Lisboa, 2829-516 Caparica, Portugal. ⁴Department of Studies in Chemistry, University of Mysore, Manasa Gangothri, Mysore, Karnataka 570006, India. ⁵Glocal School of Agricultural Science, Glocal University, Mirzapur Pole, Saharanpur District, Uttar Pradesh 247121, India. ⁶Centre for Advanced Research and Innovation, Glocal University, Delhi-Yamunotri Marg, SH - 57, Mirzapur Pole, Saharanpur District, Uttar Pradesh 247121, India. ⁷Department of Biotechnology, P. A. College of Engineering, (Affiliated to Visvesvaraya Technological University, Belagavi), Mangalore, Karnataka 574153, India. ⁸Civil Engineering Department, College of Engineering, King Khalid University, 61421 Abha, Saudi Arabia. ⁹School of Civil Engineering and Architecture, Institute of Technology, Dire-Dawa University, 1362 Dire Dawa, Ethiopia. [™]email: akheelahmed54@gmail.com; wkhan9450@gmail.com

Textiles are essential to daily human existence. Numerous phases, including production, distribution, usage, recycling, and agriculture, are involved in the entire life cycle of textiles. Political and societal attention has been focused on manufacturing and consuming textiles that influence the environment. Research on how textiles affect freshwater resources found that producing raw materials, wastewater emissions from processing textiles, and maintenance of finished products have the greatest consequences¹. Sustainable development breaks links with water use and wastewater disposal to optimize economic growth². As a result, water is a significant issue, a barrier, and a pathway for the long-term growth of businesses that generate wastewater with high levels of dangerous and toxic substances. It is projected that among the three essential categories of freshwater consumption—agricultural, industrial, and domestic—industrial freshwater use will rise by the most significant amount, or almost 76%, between 1995 and 2025³.

Water issues are frequently intimately related to how the world economy is structured^{4,5}, which strains the water resources in the exporting regions, where there are frequently insufficient procedures for prudent water governance and conservation. These aspects have led to a new "Water Security" concept. The Sustainable Water Partnership (SWP) defines water security as "the adaptive capacity to safeguard the sustainable availability of, access to, and safe use of an adequate, reliable, and resilient quantity and quality of water for health, livelihoods, ecosystems, and productive economies." SWP advances climate resilience by improving water management and considering various socioeconomic and environmental situations, strengthening the links between food, energy, and water security^{6,7}.

By 2030, it is anticipated that the Indian textile and apparel industry will have grown at a 10% compound annual growth rate (CAGR) to reach US\$ 350 billion, according to the India Brand Equity Foundation⁸. Furthermore, India ranks third globally in terms of textile and apparel exports. India is projected to export goods worth US\$100 billion, placing it among the top five exporters in the world in several textile categories⁸.

One of India's oldest economic sectors is the textile industry. The industry is incredibly diverse, with the capital-intensive, complex mills sector at one end of the spectrum and the hand-spun and hand-woven textiles sector at the other. Intense rivalry, excess capacity, narrow profit margins, and stringent environmental laws beset these sectors. Restrictions on overhead costs for wastewater treatment and research and development have affected this. Therefore, it becomes imperative to economically remove toxicity and colour from textile industrial effluents (TIE)⁸. The textile industries produce millions of tonnes of colours and myriad litres of effluent, making them the most significant users of synthetic dyes⁹. The dyes are so designed that physical, chemical, or biological agents cannot fade them. As a result, the variety of dye structures and other components found in industrial effluent make dye removal challenging. As such, they are immune to degradation and destruction by standard treatment procedures. The textile industry releases undesirable colour emissions that negatively affect the environment and public health.

The textile or fashion/apparel industry is the third most polluting industry, accounting for around 10% of the world's annual carbon footprint. According to the United Nations Environment Program (UNEP), the industry uses 93 trillion litres of water annually and is the second-biggest consumer of water¹⁰. The adoption of unsustainable and inappropriate practices in the textile industry in many countries has led to a technology gap, creating a pressing environmental challenge. It is crucial to explore and identify more effective methods to devise sustainable solutions for using recycled textile industrial effluent and reduce the textile industry's water footprint.

A significant advancement in the development of techniques, strategies, and metrics for determining freshwater appropriation and evaluating wastewater discharge from businesses and related sectors, including household sewage, is the water footprint (WF). The WF measures the amount of freshwater that humans have appropriated and contaminated. It allows us to gather unbiased data and assess the extent of the harm caused by human activity. The water footprint is divided into three sections: green, blue, and grey. Together, these components provide a comprehensive picture of water use by determining the type of water source—surface/groundwater, rainfall, or soil moisture—and the quantity of freshwater required to absorb pollutants^{11,12}.

The textile industry uses around 70% of commercial synthetic dyes that are azo dyes with a nitrogen double bond $(-N=N-)^{13,14}$. The reputation of azo dyes can be endorsed due to their medium-to-high fastness qualities, high molar extinction coefficient, significant structural diversity, ease and affordability of synthesis¹⁵. Due to their carcinogenic and mutagenic qualities and their resistance to biodegradation, textile businesses struggle to remove dye hues¹⁶.

The textile industry uses Acid Blue 113 (AB113) dye to colour wool, silk, and polyamide fibres. The dye is classified as a benzidine-based bisazo anionic dye¹⁷. It might eventually be converted into benzidine, which is known to cause cancer in people¹⁸. The textile industry utilizes the more AB113, the more health issues it will cause. Therefore, reducing the environmental impact of AB113 from textile effluents is essential. There are currently very few published reports on the adsorption, degradation, and decolourization of AB113 from water. Photo-catalytic degradation, low-frequency ultrasound-assisted degradation, electrocoagulation, and physical approaches employing UV light, nanomaterials, and inorganic materials such as activated carbons are some categories under which the presented techniques, methods, and processes. The high cost of plant establishment,

higher operating costs, regeneration problems, and related technological issues include residual sludge disposal, secondary pollutants, sensitivity to changes in waste input, interference by wastewater constituents and financial disadvantages of the techniques^{19,20} above.

Using clay as an adsorbent has recently brought dye removal from wastewater to light^{21,22}. Its low cost, wide availability, high adsorption rate, non-toxicity, and potent ion exchange capacity set it apart from other adsorbents. These features result from the mineral structure's net negative charge. Utilizing the clays can benefit the wastewater industry both environmentally and economically.

Many studies have examined the adsorption of organic cationic dyes by clay minerals²³. However, there isn't much data on anionic dye adsorption²⁴. Due to the weak interactions between the azo dyes' anionic charge and the clay minerals' surface negative charge, acidic dyes often have a lower adsorption capacity than basic dyes.

The word "nanoclay" is a broad term for mineral clays having surfaces measuring at least 50–150 nm and phyllosilicate or laminar structures in the order of nm. Even though nanoclay is frequently utilized, it's important to remember that not all its dimensions are nanoscale. Specific clay dimensions of montmorillonite laminar, which is nano in one laminar dimension but micro in the other, are categorized as nano clay but are micro size because of agglomerations or their structure. The mineral base is hydrophilic and can be either natural or manufactured.

A potential adsorbent for removing several components from industrial wastewater is halloysite nanoclay (HNC). The composition and structure of HNC is very similar to kaolinite. The mechanical stability of the soil column can be enhanced by interactions between larger HNC particle sizes, which are present in soils and sediments like kaolinite and similar minerals. HNC's adsorption capacity is determined by its edges and surface structure^{25,26}. The changing charges on the edges can be correlated using the response of the clay surface, the ions in the aqueous solution, and the ionizable surface groups on the edges. The first study on the clay-based adsorption removal of AB113 dye from water using HNC is presented in this work.

Replacing charcoal, widely used in other industries, is one of the study's goals. The high cost and E-factor of charcoal for material regeneration severely limit its potential as an adsorbent²⁷. Thus, replacing charcoal will satisfy the need for a long-term remedy for the industrial wastewater cleanup of textiles. The suggested methodology also provides a modelling approach for managing water footprints.

For the first time, our Research School used Nutraceutical Industrial Spent (NIS) as a filler material^{28,29} to fabricate thermoplastic and thermoset composites and an efficient adsorbent for dye remediation^{30–32} from TIE. Additionally, despite the large body of research showing how low-cost agricultural waste may be utilized as a biosorbent to detoxify dangerous dyes, the usage of dye-adsorbed biosorbent, or "sludge"³³, is first to our research school.

The current work investigates HNC's porosity characteristics as a superb, readily available adsorbent to clean up the hazardous dye AB113 from aqueous water and TIE. The proposed HNC as an adsorbent has a principal advantage over others regarding better adsorption capacity over many reported in the literature, a wide range of pH, and the cost-effectiveness of the commercial grade HNC as it is readily available in the market. There is no risk of deterioration and/or degradation of the material, unlike the Nutraetuical Industrial Spent reported in the literature. HNC has a long shelf life, is readily available, reasonably cheap and does not require pretreatment. Moreover, there is a shortage of knowledge on the adsorptive remediation technique for removing colour from industrial effluents and aqueous water and how to dispose of the dye-adsorbed adsorbent, generally identified as "sludge"—the current study aimed to treat textile effluents using adsorption and HNC. One of the future areas of this study was to create composites using plastic waste and dye-adsorbed HNC ("sludge"), a leftover resource, as filler and support to fit within the Circular Economy (CE) concept³³. This concept aims at eliminating waste and the continual use of waste as a resource(s) for other processes.

Experimental Materials

Determination of purity of commercial sample of Acid Blue 113

Synthetic compounds, by-products, intermediates, and unreacted starting ingredients are frequently found in commercial azo dyes. The volatility, polarity, and molecular weights of the constituents in these mixes can differ significantly³⁴. Sometimes, supposedly pure pigments include significant levels of contaminants³⁵.

The dye Acid Blue 113 (AB113), also known as Neural Blue 5R, with an empirical formula $C_{32}H_{21}N_5Na_2O_6S_2$; CAS Number: 3351-05-1; molecular weight 681.65; colour index number 26360; λ_{max} 566 nm has ϵ (extinction coefficient) \geq 18,000 at 563–569 nm in H_2O at 0.02 g L^{-1} for 50% dye content³⁶. Figure 1 depicts the dye's molecular structure.

Fig. 1. Structure of Acid Blue 113 dye.

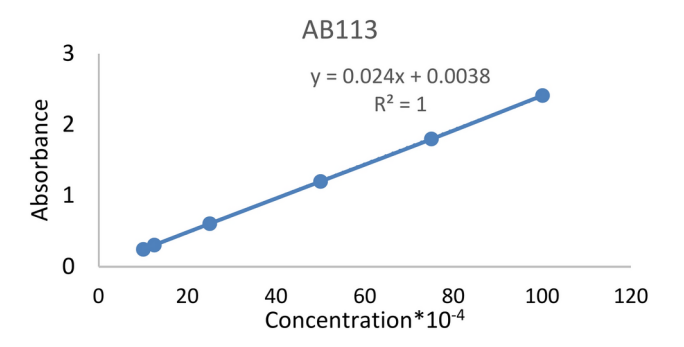


Fig. 2. Determination of molecular extinction coefficient of AB113 dye.

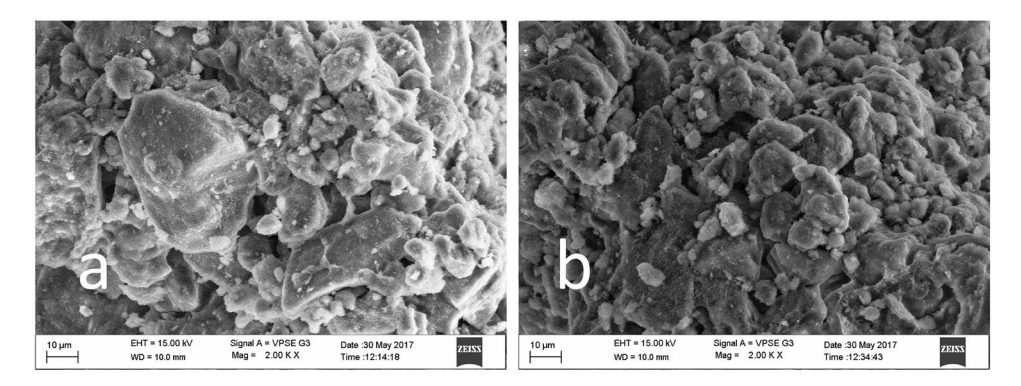


Fig. 3. (a) SEM image of HNC. (b) SEM image of AB113 dye adsorbed HNC.

The following procedure was used to determine the dye concentration of a commercial sample of AB113 used in the experiments: Six distinct concentrations $(1.00 \times 10^{-4}; 1.25 \times 10^{-4}; 2.50 \times 10^{-4}; 5.00 \times 10^{-4}; 7.50 \times 10^{-4})$ 10.00×10-4) of AB113 were made in distilled water. The absorbance was measured at 566 nm using distilled water as a reference. Plotting absorbance against concentration was done. For a route length of 1 cm, ε was determined by measuring the slope of the linear part of the curve or by applying the formula $\varepsilon = A/cl$, where A is the specific absorption coefficient for concentration c (mol L⁻¹). The absorbance's per unit path length and unit concentration are known as the specific absorption coefficient or absorbency index (Fig. 2). For the latter, the mean of six values was used to get the commercial sample's ϵ_{AB113} : $\epsilon_{AB113} = \epsilon_1 + \epsilon_2 + \epsilon_3 + \epsilon_4 + \epsilon_5 + \epsilon_6 / 6 = 2450 + 2440 + 2424 + 2402 + 2396 + 2411 / 6 = 2421.$ From the determined ϵ

value, the purity of the commercial grade AB113 was calculated.

Adsorbent preparation and characterization

HNC was purchased from India's Sigma Aldrich. The HNC was dried at 60°C for approximately 12 h, and the dried sample was employed in adsorption experiments.

Statistical optimization of process parameters

A study was done on variables including contact time (A), temperature (B), initial dye concentration (C), adsorbent dose (D), and initial pH (E) that affect the adsorption process and final adsorption capacity. At 165 rpm, the dependent response variables for stationary orbital shaking and adsorption capacity were the optimization focus for these independent variables. An equation for general quadratic regression was obtained by analysis of variance. Surface and contour plots were used explicitly to depict the effects of the parameters, both alone and in combination, on the adsorption ability.

Results and discussion Surface characterization of the adsorbent

The surface of the HNC showed a relatively porous structure when examined with a SEM (Fig. 3a). A thin adsorbate layer filled some pores after the AB113 dye was adsorbed (Fig. 3b), covering the particle. The HNC IR spectra revealed that the adsorbed water molecule and hydroxyl groups are responsible for the bandwidth observed in the IR spectrum between 3353 and 3454 cm⁻¹ (Fig. 4). C-H stretching is responsible for a sharp band at 2852 cm⁻¹, while C-O stretching is accountable for a band at 1598 cm⁻¹. Moreover, the C-O-C stretching is responsible for the 1418, 1404, 1355, 1158, and 1091 cm⁻¹ bands. According to the infrared spectrum, the broad bands between 3353 and 3454 cm⁻¹, which are the hydroxyl groups of HNC, and between 3300 and 3500 cm⁻¹,

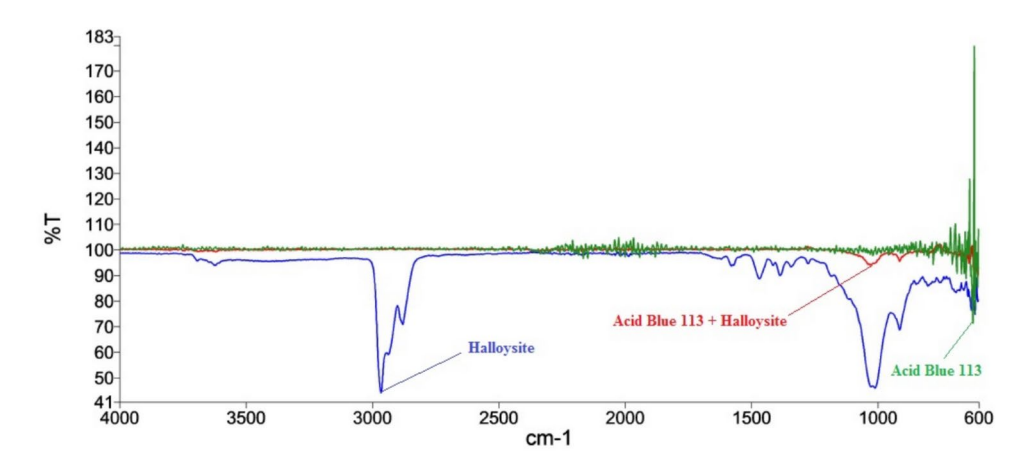


Fig. 4. Adsorption FTIR spectral analysis.

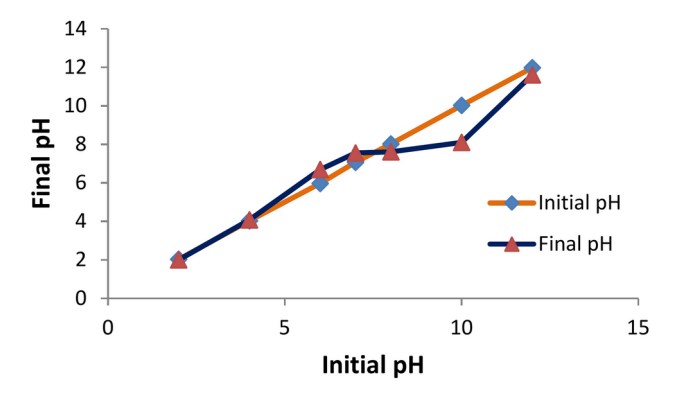


Fig. 5. Point of Zero-Charge of HNC.

which are brought on by the AB113 dye's $-\mathrm{NH}_2$ group's N–H stretching, have disappeared once the dye has been adsorbed on HNC. This finding supports the -NH2 and hydroxyl groups that form hydrogen bonds.

Furthermore, a significant peak for N–N stretching at 1598 cm⁻¹ disappearing indicates that AB113 dye has substantial adsorption on HNC. Lastly, it concludes that AB113 dye has mainly adsorbed on HNC based on decreased IR absorption frequencies. The adsorbent surface bears no charge at pH 7.60, as seen by the point-of-zero charge established at the intersection of two curves (Fig. 5).

Batch adsorption studies

Effect of pH and initial dye concentration

It is imperative to ascertain each parameter's ideal state to achieve maximal adsorption. The most crucial factor in the adsorption process is pH, which alters the ionic dye formed in the solution and the surface characteristics of the adsorbent, hence regulating the adsorption capacity. At an initial concentration of 100 mg L⁻¹, the highest AB113 dye elimination by HNC occurred at pH 2.0 (q_e = 95.00 mg g⁻¹) (Fig. 6a). As seen in Fig. 6b, the q_e value rises as the initial dye concentration surges from the variety of 25–100 mg L⁻¹. The percentage q_e value rose as concentration increased, reaching a maximum in the concentration solution's 25–100 mg L⁻¹ range. After that, as concentration increases, the percentage q_e value drops.

Effect of adsorbent dosage

Given the operating conditions, the adsorbent dose determines the adsorption capacity for the adsorbate's initial concentration. It has a substantial influence on the adsorption method. In the range of 0.500–6.000 g, the effect of the adsorbent dose on AB113 dye adsorption was examined. It was revealed that as the adsorbent dosage amplified, so did the percentage of AB113 dye elimination. A larger dose of adsorbent improved the transfer of AB113 dye to HNC. Any additional adsorbent dose increase after the limit had no discernible effect on the adsorbate yield. Nearly all dye molecules adhere to the adsorbent surface, causing the dye molecules in the solution and the adsorbent to reach equilibrium. The findings are displayed in Fig. 6c.

Effect of contact time on dye adsorption

We gave the AB113 dye 15, 30, 45, 60, 90, 120, 150, and 180 min to adsorb onto HNC. 60% of the total amount of adsorption happened in the first 15 min, indicating fast adsorption. Nevertheless, a gradual rise in adsorption

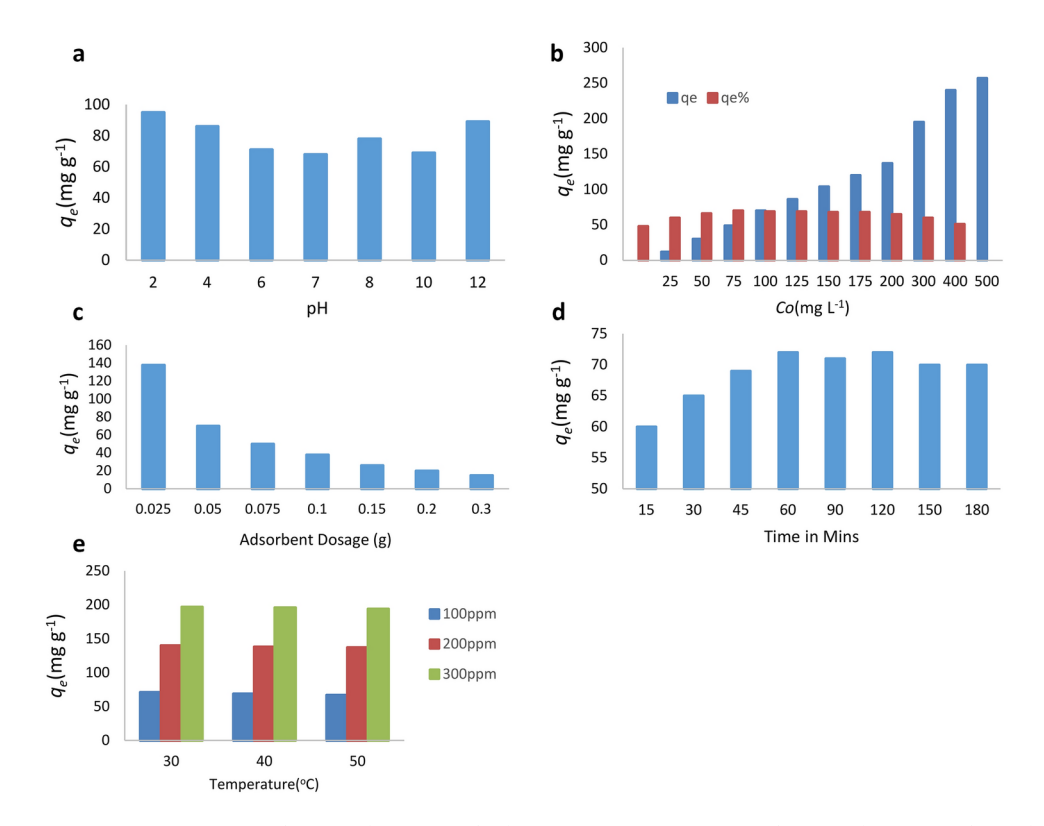


Fig. 6. (a) Parametric effect on adsorption of solution pH. (b) Parametric effect on adsorption of initial dye concentration. (c) Parametric effect on adsorption of adsorbent dosage. (d) Parametric effect on adsorption of contact time. (e) Parametric effect on adsorption of temperature.

was observed as the duration of contact increased, lasting until 60 min and gradually reaching equilibrium, as depicted in Fig. 6d. Dye molecules diffuse deeper and with more incredible energy into the adsorbent structure as they aggregate with longer contact times. Because the mesopores fill up and begin to provide resistance to the diffusion of aggregated dye molecules in adsorbents, this aggregation eliminates the effect of contact time.

Effect of temperature

Temperature is another aspect that impacts the adsorption course. The results of adsorption experiments using three different dye concentrations at 30–50 °C are shown in Fig. 6e. The nominal variation of adsorption with the range of temperature studied onto the surface of HNC may be due to minimum variation on the rate of intra-particle diffusion phenomena, and the dye molecule's mobility with a drop in kinetic energy may cause temperature-independent adsorption³⁷.

Adsorption isotherms

The characteristics of adsorption isotherms are essential for comprehending the exchanges between adsorbate molecules and the adsorbent surface. Adsorption isotherm models are utilized to understand the adsorption of AB113 dye onto HNC. The Freundlich and Langmuir isotherms are two popular models for estimating adsorption capacity and fitting experimental data. When an adsorbent surface has a restricted number of equal adsorption sites with unvarying energies, monolayer adsorption occurs according to the Langmuir isotherm model³⁸. The initial AB113 dye doses of 25–500 mg L⁻¹ were used in the equilibrium studies. Comparing this isotherm's Q_m value of 631.09 mg g^{-1} to the trial q_e value of 95.00 mg g^{-1} , it is very high.

On the other hand, the R^2 value of 0.84 shows that this isotherm fits the trial data quite well. For the Langmuir isotherm, the separation factor R_L is significant³⁹. The computed R_L values ranged from 0.332 to 0.908, suggesting that the AB113 dye adsorbed favourably onto HNC. Adsorption is more advantageous at high concentrations, as evidenced by the decrease in R_L value with rising starting concentration. The authors looked into alternative adsorption isotherm approaches because of the significant discrepancy between Q_m (631.09 mg g⁻¹) and q_e (95.00 mg g⁻¹). Adsorption on a heterogeneous surface is hypothesized using an empirical formula called the Freundlich isotherm model⁴⁰. According to the results of this investigation, the adsorption is physisorption and favours the standard Langmuir isotherm with n_F and $1/n_F$ values of 1.267 and 0.789, respectively. A correlation coefficient R^2 value of 0.96, obtained by fitting the Freundlich isotherm to the experimental data, indicates that the process is linear. It is possible to deduce that AB113 adsorbs onto HNC in a physisorption mechanism that is advantageous for the experimental setup. Since the Langmuir and Freundlich models failed to identify whether the system is homogeneous or heterogeneous conclusively, the authors have investigated higher models to suit the data (Fig. 7a). The Jovanovic isotherm is a development of the Langmuir isotherm model⁴¹. The Jovanovic isotherm yielded a high Q_m value of 374.06 mg g^{-1} , higher than the trial value of q_e , which is 95.00 mg g^{-1} . As

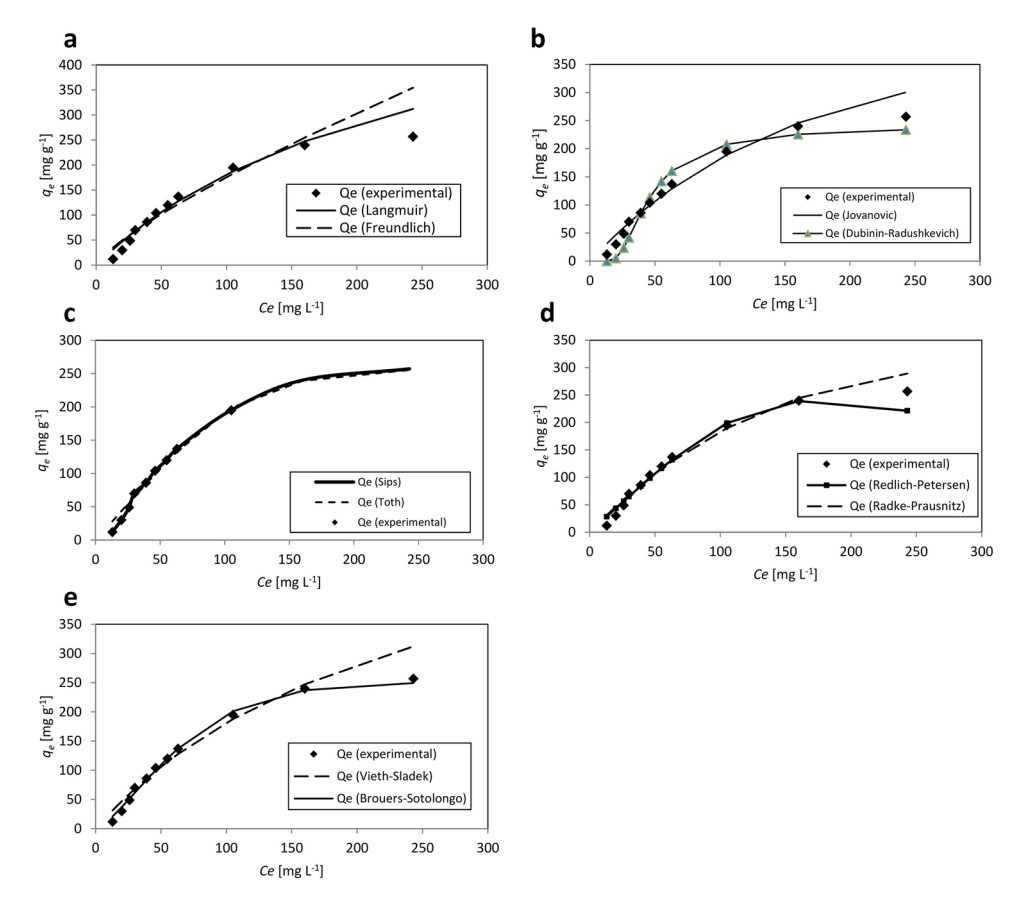


Fig. 7. (a) Data fit of experimental and various isotherms adsorption models. (b) Data fit of experimental and various isotherms adsorption models. (c) Data fit of experimental and various isotherms adsorption models. (d) Data fit of experimental and various isotherms adsorption models. (e) Data fit of experimental and various isotherms adsorption models.

Langmuir		Freundlich		Jovanovic		Dubinin-Radushkevich		
Q_m	631.09	K_F	4.65	Q_m	374.06	Q _s 240.29		
K_{S}	0.004	n_F	1.267	K _J	0.007	K _{ad} 0.0002		

Table 1. Calculated isotherm parameters for two limitations.

Redlich- Peterson		Toth		Radke- Prausnitz		Sips		Vieth- Sladek		Brouers- Sotolongo	
A _{RP}	2.2	Q_m	261.5	Q_m	576,200.4	Q_m	358.7	Q_m	630.1	Q_m	250.7
B_{RP}	6.12E-07	n_{T0}	3.506	K_{rp}	4.3E-06	Ks	0.048	K _{vs}	1E-07	K _{BS}	0.002
g	2.664	b _{T0}	19,860,111	m _{rp}	701.963	m _s	3.367	β_{VS}	0.004	α	1.398

 Table 2. Calculated isotherm parameters for three limitations.

a result, the value of the Jovanovic model is closer to the trial q_e value than the Langmuir isotherm. Another empirical model was the Dubinin-Radushkevich isotherm⁴², which uses a pore-filling appliance for adsorption. The Dubinin-Radushkevich isotherm yielded a q_s value of 240.29 mg g⁻¹, more significant than the experimental value. The correlation coefficient (R^2) value of 0.97 obtained by fitting the Dubinin-Radushkevich isotherm to the trial data indicates that the process is linear. It fits data slightly better than the Langmuir model because of its similarity in χ^2 and R^2 values (Fig. 7b). Tables 1, 2, and 3 display the findings of Langmuir and Freundlich, which indicate that the AB113 dye's interaction with HNC is linear, favourable, and physical. Six additional isotherm models with three parameters—Toth, Sips, Radke-Prausnitz, Redlich-Peterson, Vieth-Sladek, and Brouers-Sotolongo—were also examined for scholarly purposes.

Isotherms	Langmuir	Freundlich	Jovanovic	Dubinin-Radushkevich	Redlich-Peterson	Toth	Radke-Prausnitz	Sips	Vieth-Sladek	Brouers-Sotolongo
SSE	1042.3	1831.5	959.6	4220.8	612.4	588.9	911.4	101.4	1042.3	273.3
χ^2	42.205	65.145	43.705	66.571	30.308	29.750	42.791	2.018	45.205	9.843
R^2	0.98	0.96	0.98	0.97	0.99	0.99	0.99	0.99	0.98	0.99

Table 3. Statistical factors for model fitting.

Initial Concentration	Temp		Pseudo-F	irst-Order		Pseudo-Second-Order				
[ppm]	[K]	$\begin{bmatrix} Qe_{expt} \\ [\text{mg g}^{-1}] \end{bmatrix}$	$\begin{bmatrix}Qe_{pred}\\[\text{mg g}^{-1}]\end{bmatrix}$	k_1	\mathbb{R}^2	χ^2	$\begin{bmatrix} Qe_{pred} \\ [\operatorname{mg}\operatorname{g}^{-1}] \end{bmatrix}$	k_2	R ²	χ ²
	303	71	66.33	2.22E-01	0.51	0.53	69.92	7.45E-03	0.80	0.62
100	313	69	65.77	2.54E-01	0.56	0.24	68.28	1.10E-02	0.85	0.08
	323	67	63.50	2.82E-01	0.40	0.26	65.57	1.40E-02	0.71	0.12
	303	140	135.42	2.83E-01	0.49	0.38	139.57	6.90E-03	0.82	0.14
200	313	138	132.78	1.33E+02	0.44	0.38	65.88	1.71E-03	0.76	1.65
	323	137	132.00	2.86E-01	0.48	0.34	135.89	7.37E-03	0.81	0.13
	303	197	190.49	3.50E-01	0.31	0.30	193.90	8.97E-03	0.63	0.16
300	313	196	190.31	3.36E-01	0.37	0.30	194.00	8.13E-03	0.70	0.15
	323	194	188.50	1.06E+00	0.35	0.37	192.79	9.21E-03	0.72	0.10

Table 4. Models of absorption kinetics parameters that predict theoretically and found experimentally.

Another empirical equation created to represent systems for heterogeneous adsorption and progress the fitting of the Langmuir isotherm is the Toth isotherm 43 . The Q_m value of 261.50 mg $\rm g^{-1}$ is more than the trial q_e value of 95.00 mg $\rm g^{-1}$ and less than the Langmuir isotherm value of 631.09 mg $\rm g^{-1}$, as shown in Table 3 and Fig. 7c. The combination of the Freundlich and Langmuir isotherms is known as the Sips isotherm 44 . At low adsorbate concentrations, the Freundlich equation replaces the Sips equation. The formula provides the Langmuir isotherm's typical monolayer adsorption capacity at high adsorbate concentrations. Compared to the value obtained for the Langmuir isotherm, the value of Q_m = 358.70 mg $\rm g^{-1}$ obtained for the Sips isotherm has more variation than the experimental value. It fits the experimental data relatively well, with lower SSE (101.40), χ^2 (2.018), and higher R^2 (0.99) values that are close to the Langmuir model.

The estimated value is recommended to closely resemble the experimental value to achieve optimal fitting of the isotherm model and a well-balanced Q_m prediction. A smaller χ^2 value indicates more agreement with the experimental results (Fig. 7d). However, a predicted Q_m of 576,200.40 mg g $^{-1}$ was derived using the Radke-Prausnitz isotherm 45 , much higher than the Q_m value measured experimentally. With a correction exponent of "g," the Redlich–Peterson isotherm model 46 was shaped to improve the fitting of the Langmuir–Freundlich equations. The obtained "g" value of 2.664 shows that the adsorption is leaning toward the Langmuir isotherm. The Vieth-Sladek isotherm 47 was initially used to describe solutes adsorbed by a particular isotherm that streamlines a nonlinear component (Langmuir equation) and a linear component (Henry's law). The nonlinear component illustrates how solutes adhere to specific spots on porous adsorbent surfaces. The linear component and the solute dispersed in the amorphous areas of the adsorbent polymers have a physical correlation. We compared the anticipated Q_m value of 631.10 mg g $^{-1}$ to other models under study.

The Vieth-Sladek isotherm model forecasts diffusion rates in solid materials based on transient adsorption.

The Vieth-Sladek isotherm model forecasts diffusion rates in solid materials based on transient adsorption. The Vieth-Sladek isotherm and the Brouers-Sotolongo isotherm⁴⁸ are comparable. This isotherm yielded a Q_m value of 250.70 mg g^{-1} , more significant than the experimental value of 95.00 mg g^{-1} . Nonetheless, this isotherm model's R^2 value 0.92 accurately predicts the trial data (Fig. 7e). These models are of higher-order equations and are utilized to comprehend the adsorption appliance. Since R^2 value only applies to linear models, it cannot confirm the accuracy of data fitting. Since χ^2 would be low if the model and experimental data were comparable, and vice versa, χ^2 values offer a better indicator. As indicated in Tables 3 and 4, values for the essential parameters were obtained from all nine isotherm models (Q_m, χ^2) , and R^2 . Researchers studying mathematical modelling, in particular, will be interested in the difference in values found for the experimental values and parameters of every model under study (q_e) . These researchers may be able to develop new models to understand better the phenomenon of adsorption in the AB113-HNC system.

Adsorption kinetics

Kinetic models are analyzed to determine possible rate-controlling phases in the adsorption development. AB113 dye was employed at 75, 150, and 300 ppm concentrations for the kinetic investigations. Kinetics investigations at three different temperatures (303 K, 313 K, and 323 K) provide information about the variation in the adsorption rate. Nonlinear analysis was used to examine the adsorption kinetic data (MS Excel 2010) employing pseudo-first order⁴⁹, pseudo-second order⁵⁰, and intraparticle diffusion by Weber-Morris model²¹. Additionally examined were the Dumwald-Wagner model⁵¹ and the Film Diffusion model⁵². Tables 4 and 5 present the estimated parameters.

Initial concentration	Temp	Film diffusion model		Weber-Morris model	Dumwald- Wagner		
[ppm]	n] $ \mathbf{K} \mathbf{R}^{ }[\mathbf{min}^{-1}] \mathbf{R}^{2} \mathbf{k}_{ist}^{ }[\mathbf{mg} \mathbf{g}^{-1} \mathbf{s}^{-0.5}] \mathbf{R}^{2} $		K [min ⁻¹]	R ²			
	303	0.0446	0.89	2.18	0.98	0.043	0.89
100	313	0.0406	0.96	1.54	0.99	0.040	0.96
	323	0.0379	0.90	1.33	0.95	0.037	0.89
	303	0.0509	0.96	2.58	0.98	0.050	0.96
200	313	0.0472	0.90	2.46	0.98	0.046	0.90
	323	0.0468	0.91	2.44	0.99	0.046	0.91
	303	0.0430	0.75	2.29	0.91	0.042	0.75
300	313	0.0470	0.86	2.43	0.94	0.046	0.86
	323	0.0474	0.93	2.14	0.96	0.048	0.93

Table 5. Models of diffusion parametric calculation.

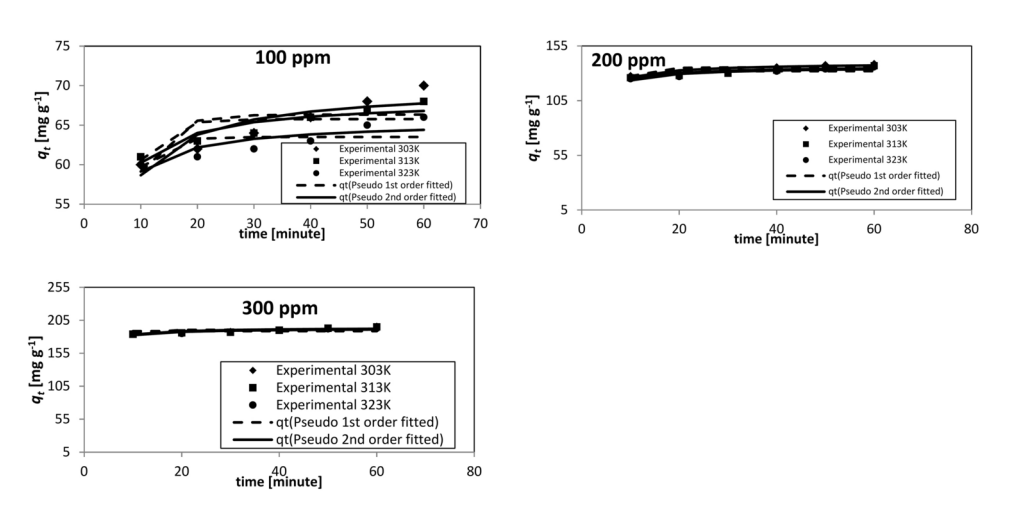


Fig. 8. (a) 100 ppm initial concentration of AB113 dye on HNC system at unlike temperatures. (b) 200 ppm initial concentration of AB113 dye on HNC system at unalike temperatures. (c) 300 ppm initial concentration of AB113 dye on HNC system at unlike temperatures.

The pseudo-second-order model outperformed the pseudo-first-order model in fitting the experimental data at initial AB113 dye concentrations of 100, 200, and 300 ppm at various temperatures, according to coefficients of determination (R^2) and chi-square values (χ^2) (Fig. 8a, b, and c). Once maximum adsorption was reached, the fast adsorption rate steadily reduced to become stationary. The temperature, in the range studied, has limited influence on the adsorption capacity (q_e). This property also helps during the valorization process. These findings demonstrate that the adsorption processes bring on no rate constraint. The results further indicate that during the adsorption process, the solute molecules diffused into the pores of the HNC after moving from the bulk solution to the solid surface.

The Dumwald-Wagner model (Fig. 9a) is used to compute the fundamental absorption rate constant (K), which is then modified for experiential diffusion effects (Table 5). The Weber-Morris model (Fig. 9b) shows that the solute uptake changes with $t^{1/2}$, as opposed to the time of contact (t). Therefore, plotting q_t vs $t^{1/2}$ should show the diffusion rate constant (k_{int}) as a straight line that crosses the origin. A single process does not always govern the kinetics of adsorption. Our experimental data clearly shows that many degrees of linearity exist at all solute concentrations. The adsorption rate rises at lower starting concentrations (100 ppm) and lower temperatures. After that, the rate travels in a different linear direction until reaching a time-dependent equilibrium. At higher temperatures, though, the rate becomes more linear. When the film diffusion model fits data at higher temperatures, the solute concentration (300 ppm) results in less pronounced changes in the adsorption rate. Based on the data in Fig. 9c, we may deduce that high adherence to the model yields a liquid film diffusion constant R' (Table 5) with high R^2 and χ^2 values. These values imply that diffusional restrictions result in a minor blockage rate due to adsorption at higher temperatures. We can conclude that diffusion is a mechanism that sets a rate limit. The solute is first quickly absorbed onto the particle's surface, creating a coating to change the absorption rates and postpone additional diffusion,

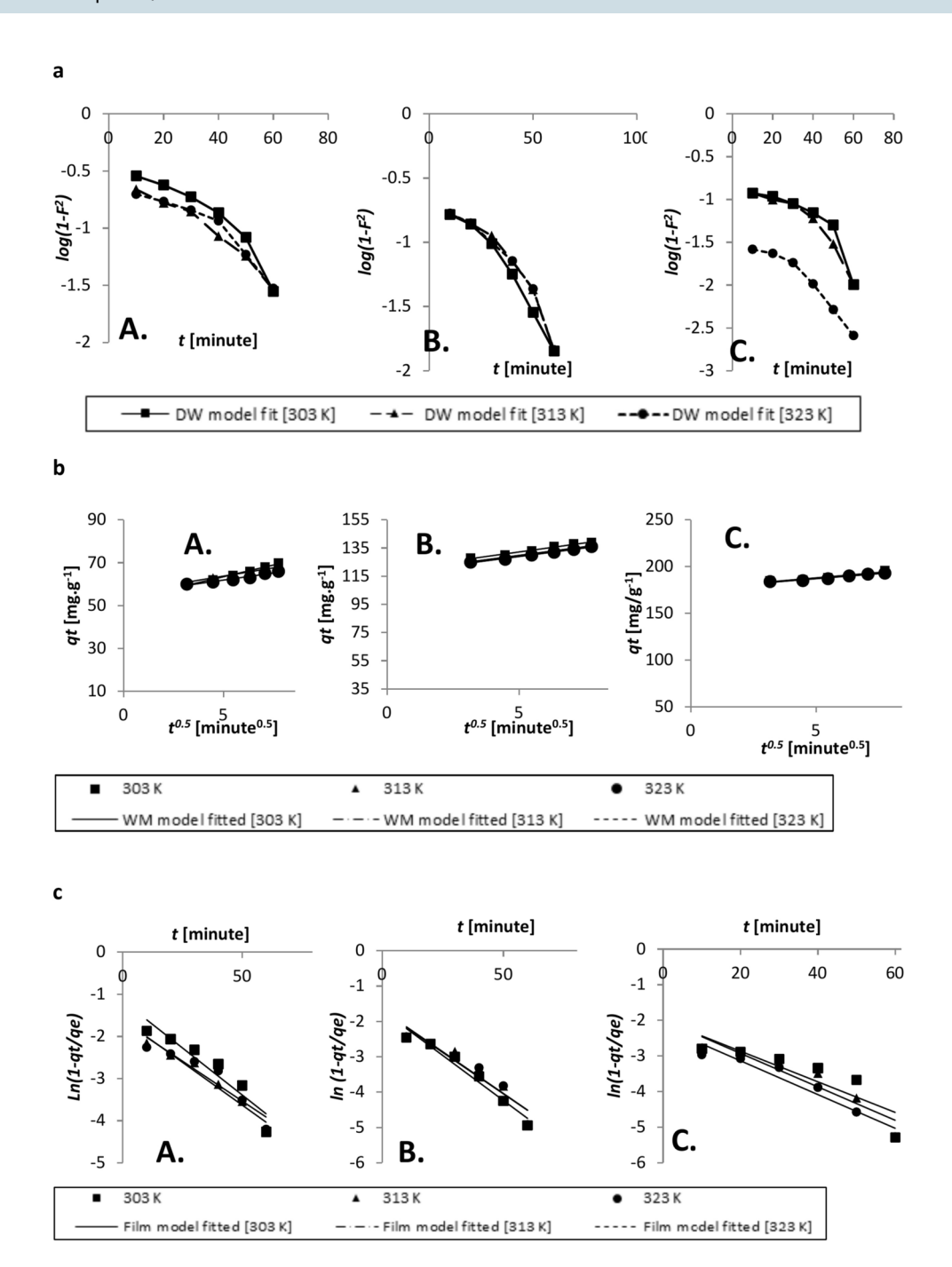
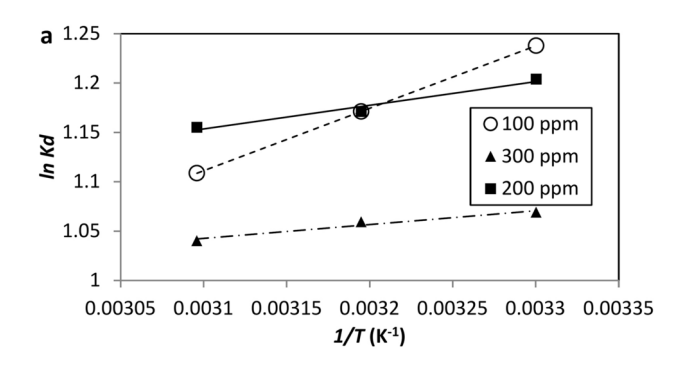


Fig. 9. (a) Dumwald-Wagner model: A) 100 ppm, B) 200 ppm, C) 300 ppm. (b) Weber-Morris model: A) 100 ppm, B) 200 ppm, C) 300 ppm. (c) Film diffusion model: A) 100 ppm, B) 200 ppm, C) 300 ppm.

Adsorption thermodynamics

Energy and entropy are the main aspects to be considered when planning the interaction process. The standard Gibbs free energy change (ΔG°) is typically used to quantify the spontaneity of the adsorption process. Significant adsorption occurs when the free energy change (ΔG°) of adsorption is negative. As illustrated in Fig. 10a and b, the slope and intercept of the Van't Hoff plots of $\ln K_d$ and $\ln K_2$ vs 1/T can be used to calculate ΔH° , ΔS° , and E_d .

Table 6 presents estimations of the thermodynamic constraints. The adsorption process appears feasible and spontaneous when the ΔG° is negative, and the ΔH° value is positive, indicating adsorption's endothermic nature. For every temperature under investigation, the ΔG° is negative, suggesting that the adsorption of AB113 dye onto HNC proceeds almost spontaneously and advantageously. As the temperature rises, the ΔG° value drops, suggesting that adsorption increases at higher temperatures. A positive value for ΔS° indicates that the AB113 dye has a good affinity for the adsorbent and that the solid solution's surface is more randomly distributed. The shallow values of ΔH° suggest that the adsorption mechanism is physical, as the standard enthalpy change for a chemical reaction is > 200 kJ mol⁻¹. The results are further supported by the activation energy values of the



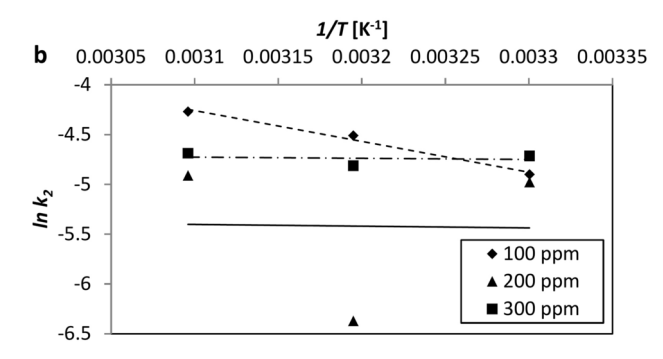


Fig. 10. (a) Thermodynamic constant at equilibrium v/s 1/T. (b) Kinetic constant of pseudo-second-order v/s 1/T.

Initial concentration	Temperature	ΔG°	ΔS°	ΔH°		Ea
[ppm]	[K]	[kJ mol ⁻¹]	[J mol ⁻¹ K ⁻¹]	[kJ mol ⁻¹]	ln A	[kJ mol ⁻¹]
	303	- 3.12				
100	313	- 3.05	- 7.06	- 5.26	5.33	25.72
	323	- 2.98				
	303	- 3.03				
200	313	- 3.05	3.42	- 1.99	- 4.86	1.44
	323	- 3.10				
	303	- 2.69				
300	313	- 2.76	5.06	- 1.16	- 4.36	0.98
	323	- 2.79	1			

Table 6. AB113-HNC thermodynamic structures.

adsorption process at 100, 200, and 300 ppm of initial concentrations using the Arrhenius equation and the kinetic constant from the pseudo-second-order model. These values ranged from 0.98 to 25.72 kJ mol $^{-1}$.

Statistical optimization by fractional factorial experimental design

Response surface methodology (RSM) is a collection of statistical and mathematical techniques for developing, improving, and optimizing processes. It also has essential applications in designing, developing, and formulating new products and improving existing product designs. The most extensive applications of Response surface methodology (RSM) are in the industrial world, in developing, designing, and formulating new products, particularly in situations where several input variables potentially influence some performance measure or quality characteristic of the product or process. It is typically measured on a continuous scale. Most real-world applications of RSM will involve more than one response. The input variables are sometimes called independent variables. RSM primarily employs the statistical regression method as it is practical, economical and relatively easy to use. This polynomial model usually refers to a regression model. The second-order regression model has proved to be more effective in predicting the performance of the given data set.

We used a variety of combinations of the five independent factors in experiments to look at the effects of each independent variable by itself and in combination. The analysis of variance using quadratic regression (Table 7) clearly shows how significant each component's individual and combined effects are. We assessed factor significance at a 95% confidence interval with a p-value less than 0.05%. The remaining variables in this study are not significant, but A, C, D, AC, A², C², and D² are significant model terms. There are zero cross-products

Source	Sum of squares	Degree of freedom	Mean square	F value	p-value
Model	316,189.5	13	24,322.3	211.2	< 0.001**
A	730.4	1	730.4	6.3	0.0135*
В	13.4	1	13.4	0.1	0.7338
С	90,417.1	1	90,417.1	785.2	< 0.001**
D	6409.0	1	6409.0	55.7	< 0.001**
AB	78.2	1	78.2	0.7	0.4120
AC	18.2	1	18.2	0.2	0.6920
ВС	508.9	1	508.9	4.4	0.0383*
A ²	3365.4	1	3365.4	29.2	< 0.001**
B ²	1.4	1	1.4	0.0	0.9123
C ²	3499.5	1	3499.5	30.4	< 0.001**
D^2	2541.1	1	2541.1	22.1	< 0.001**
E ²	326.1	1	326.1	2.8	0.0958+
Residual	10,478.6	91	115.1		
Total	326,668.1	104			

Table 7. ANOVA Table. Significant figures. *Suggestive significance (p value: 0.05). *Moderately significant (<math>p value: 0.01). **Strongly significant (<math>p value: $p \le 0.01$).

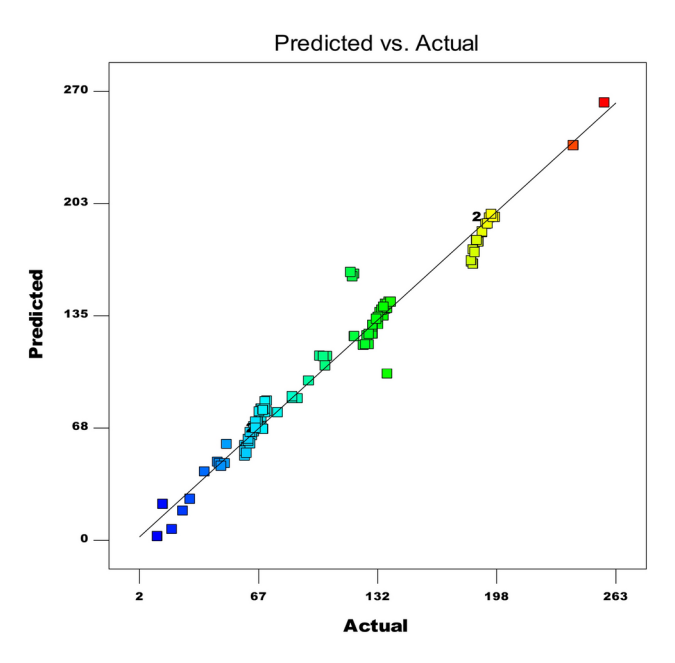


Fig. 11. Data comparative plot of actual values v/s predicted values.

for AC, AD, AE, AD, BE, BF, CD, CE, CF, and DE. The RSM model has a F-value of 211.2, making it extremely important. There is a sensible arrangement between the reformed R^2 value of 96.8% and the projected R^2 value of 80.5%. The model facilitates navigating the design space with a high coefficient of variance of 9.6% and R^2 of 95.4%. The graph that compares actual and expected values shows a strong relation between the experimental and expected replies (Fig. 11). The investigation yielded a regression equation, as shown below.

$$\begin{aligned} & \text{Adsorption} = & 120.6 + 14.7 * \text{A} - 1.5 * \text{B} + 122.9 * \text{C} - 39.2 * \text{D} - 5.3 * \text{E} - 2.6 * \text{AB} + 11.1 * \text{AC} + 3.5 * \text{BC} \\ & - 26.5 * \text{A}^2 - 0.3 * \text{B}^2 - 43.8 * \text{C}^2 + 47.2 * \text{D}^2 - 13.2 * \text{E}^2 \end{aligned}$$

To maximize the second-order polynomial equation with interaction features, we employed multiple regression analysis based on FFED to determine the optimal values of the variables. Under optimal conditions of pH 1, adsorbent dose of 0.500 g $\rm L^{-1}$, initial dye concentration of 623 mg $\rm L^{-1}$, adsorption period of 139 min with orbital shaking of 165 rpm at 49 °C, the maximum adsorption value determined by statistical optimization was 329 mg $\rm L^{-1}$. One primary reason for optimal conditions of pH 1 is that the surface of the HNC contains negative charges. The dye is likely to get protonated at low pH, and the resultant positive charge helps the adsorption process due to non-conventional bonds such as hydrogen bonds, van der Waals forces and electrostatic forces of attraction.

The pH one will have the least effect as it can be neutralized by alkali, such as NaOH, which is cost-effective and results in salt formation, which has the least impact on the environment.

The final phase in the statistical optimization process was to analyze the contour and 3D-response surface plots as a function of two independent variables.

Statistical process optimization can determine the ideal condition and the effect of the process parameters on the adsorption within a specified collection of parameter values. Time positively impacts adsorption capacity, according to three-dimensional graphs plotting time against every other variable. Increasing the temperature, duration, and dye concentration can hasten adsorption. At most, the adsorption procedure should take 139 min. However, extending the time further has been shown to improve adsorption. Temperature increases positively impact adsorption capacity. Over time, at the ideal temperature of 49 °C, adsorption ability increases in step with temperature. At a concentration of 623 mg L⁻¹, the highest adsorption capacity of 329 mg g⁻¹ was shown. Temperature positively affects the reaction with every other variable, according to graphs showing temperature against other independent variables. An increase in the starting concentration favours the adsorption capacity, per plots that plot the initial dye concentration versus other factors. Adsorption capability can be significantly raised with a higher starting dye concentration. Thus, the surface and contour plots graphically depict the combined effect of two constraints on the adsorption (Fig. 12a-g).

It has been demonstrated that the quadratic model intended for process optimization makes it easier to anticipate the maximum adsorption ability and understand the relationship among independent components and how they affect the adsorption process. Because of statistical optimization, the adsorption percentage has significantly increased from 95 to 329 mg g $^{-1}$.

Application of proposed method to textile industrial effluent [TIE]

Numerous processes used in the textile industry result in wastewater with a broad range of components containing high suspended particle concentrations, wildly fluctuating pH, abrupt changes in temperature, vibrant colour, and elevated COD levels⁵³. As a result, the matrix effect makes it challenging to identify a particular dye in industrial effluent⁵⁴. A straightforward approach was designed to remove AB113 dye from water and effluent from the textile industry. Samples of wastewater were taken from a nearby textile factory that works two shifts. The pipe's end, where the treatment plant receives the wastewater and is transferred to 10-L plastic containers, yielded six random TIE samples. Three working days were spent gradually collecting three samples from the first and second shifts. A 100-L barrel was filled with the collected textile manufacturing effluent samples, and they were manually stirred⁵⁵ to attain a consistent concentration. In Fig. 13, the filtrate solutions are shown.

Scaling up to five times the adsorbent, ten times the adsorbate, and an order of magnitude more of the solution's volume would improve results, according to a preliminary trial analysis. Compared to Solution 1, the absorbance of Solution 2 decreased by nearly 57%. This observation could result from the dye and other constituents present in TIE getting absorbed by HNC. Furthermore, it was observed that adding new adsorbent materials every fifteen minutes improved the dye removal from TIE. After 15, 30, and 45 min, we observed that the dye and related compounds had recovered to 43%, 91%, and 94% from Solution 2. The kinetic facts, which demonstrate that the solute quickly adsorbs onto the particle surface and forms a layer that reduces further diffusion and alters the absorption rates, corroborate this conclusion.

The experiment utilized 0.5 g, 1.0 g, and 5.0 g of HNC, while HDPE beakers containing 1, 2, and 5 L of Solution 2 were utilized. A magnetic stirrer was used to swirl the liquids vigorously. As indicated before, the procedure was repeated, yielding almost identical results. Every experiment was run three times, and the findings are presented as the average of the three runs. All results have coefficients of variance within $\pm 2\%$ error. In short, the experiment has demonstrated promising findings when scaled up by about three orders of magnitude from its initial setting. The original data may not fully explain several characteristics of industrial effluent, which is a significant drawback of this kind of research. A much larger pilot-scale study may be employed to target the outcomes precisely. However, given that the flaws in the procedure have been found and that the improved scale experimental facts will continue to display the technique's potential and reliability, there may be sufficient evidence that the method's principles will be helpful when implemented more widely in industry.

Regeneration of the adsorbent and cost analysis

The adsorbent regeneration allows for the improvement of the adsorbed material and the reusing of dye-loaded HNC. The process is not recommended because the cost of the solvents and the process will be significantly higher than the cost of the adsorbents used. Additionally, as the earth can no longer support any more environmental toxins, it will increase the E-factor²⁷, which is disagreeable. A different strategy presently being developed to create thermosets and thermoplastics would be one way to eliminate the waste materials from the process, and the research work is in progress.

Conclusion

The three primary basics of recycling are reuse, renewal, and recovery. These are the corrective methods used in environmental supervision. By treating hazardous dyes with HNC as an adsorbent, textile industry effluent (TIE) has been enhanced in value. HNC worked well in an aqueous solution as an adsorbent for AB113. In the quadratic model developed for process optimization, the adsorption capacity of HNC was found to be compatible with the Vieth–Sladek isotherm model. The results showed values of 329 mg g⁻¹. AB113's adsorption process was almost spontaneous. Intra-particular diffusion was greatly affected by the film, and the process was essentially physical. According to kinetic studies, the best fit is consistent with the pseudo-second-order model. Mass transfer processes were significantly influenced by intraparticle diffusion. The SEM and FTIR spectra demonstrated that AB113 was adsorbed onto HNC. This observation is essential to combat pollution, providing

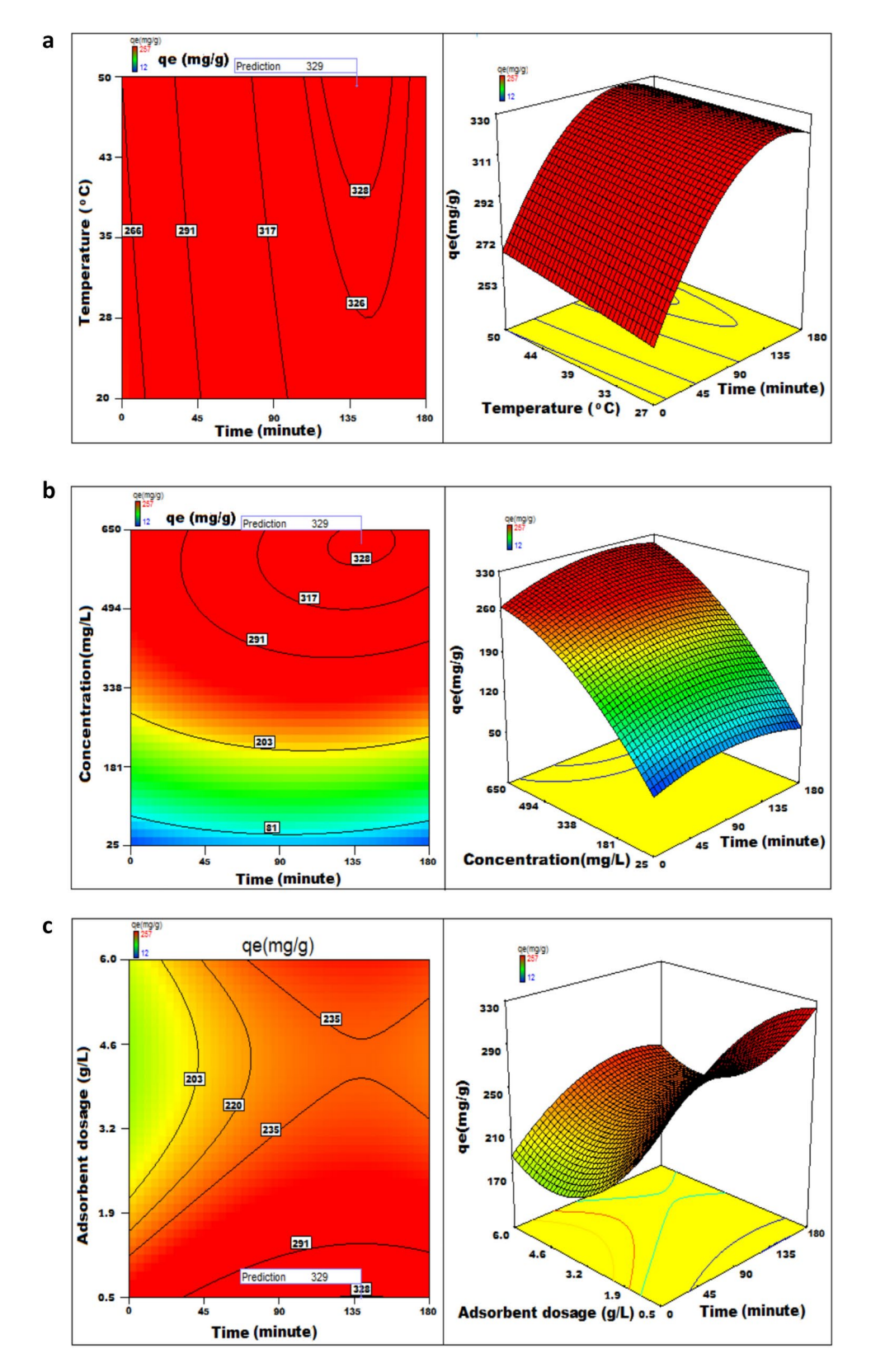


Fig. 12. (a) Adsorption capacity fluctuation with temperature versus time. (b) Adsorption capacity fluctuation with time versus concentration. (c) Adsorption capacity fluctuation with time versus adsorbent dosage. (d) Adsorption capacity fluctuation with time versus pH. (e) Adsorption capacity fluctuation with temperature versus concentration. (f) Adsorption capacity fluctuation with temperature versus absorbent dosage. (g) Adsorption capacity fluctuation with temperature versus pH.

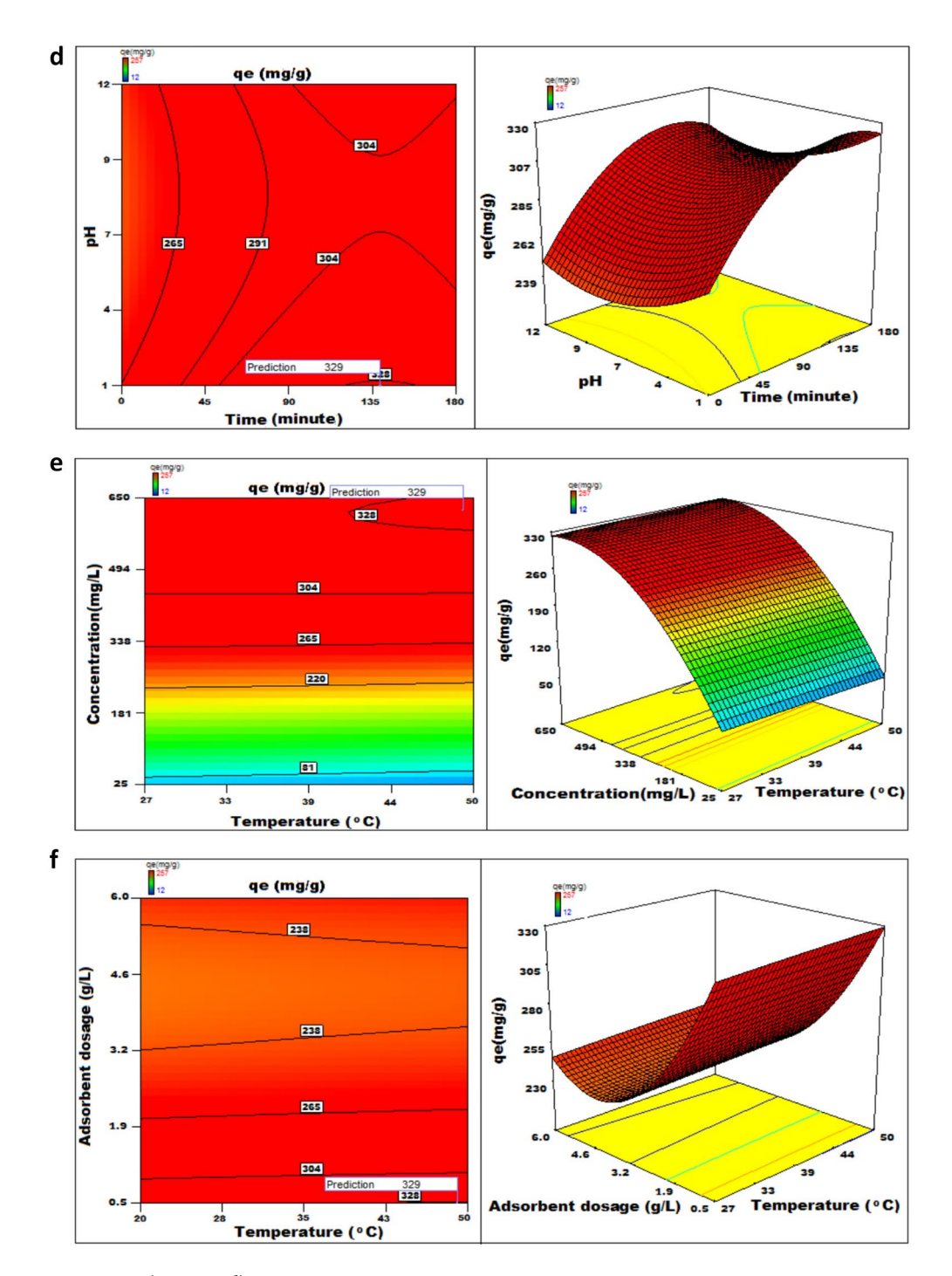


Figure 12. (continued)

a more efficient, economical, and long-lasting solution. As seen in the literature ^{56–69}, the present investigations show that greywater pollution can diminish or change grey water (TIE) into blue water.

Consequent to stricter laws, more pollution from the textile industry, and the high price of activated charcoal, readily available, reasonably priced, and easily useable clay provides an excellent alternative to activated charcoal. In the textile sector, HNC maximizes water security, minimizes E-factor, and minimizes grey water footprints as an effective adsorbent. Carbon footprints decrease when composite materials from plastic waste are fabricated using dye-adsorbed HNC "sludge" as a resource material. Furthermore, it is possible to handle the unaddressed problem of sludge disposal to meet the needs of a circular economy. We're working on it at our research school.

In conclusion, the current work offers a different paradigm by integrating the water footprint model with sustainability. If adopted commercially, the methodology will have ample economic benefits and reduce carbon and water footprints. Furthermore, our research will offer a different approach to 21st-century environmental toxins and resource depletion challenges. The authors anticipate that their project will pave new paths for green

Figure 12. (continued)

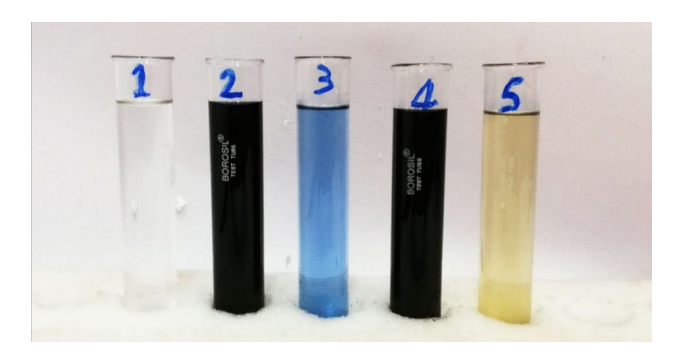


Fig. 13. Color of the solutions before and after adsorption: 1. Distilled water; 2. AB113 dye in distilled water; 3. TIE; 4. AB113 dye in TIE; 5. Filtrate after adsorption of dye on HNC after 45 min.

technology and sustainability by lowering water and carbon footprints and opening up new vistas to align with the awareness of the circular economy.

Data availability

The datasets used and/or analysed during the current study available from the corresponding author on reasonable request.

Received: 1 January 2025; Accepted: 31 March 2025

Published online: 21 April 2025

References

- 1. Morrison, J. I., Schulte, P. Water disclosure 2.0: Assessment of current and emerging practice in corporate water reporting. Pacific Institute, 2009.
- 2. Li, Y., Lu, L., Tan, Y., Wang, L. & Shen, M. Decoupling water consumption and environmental impact on textile industry by using water footprint method: A case study in China. Water 9(2), 124 (2017).
- 3. Cardone, R. Wet Business Risks. *Corporate Knights*, **2004**, *3*(2).
 4. Hanjra, M. A. & Qureshi, M. E. Global water crisis and future food security in an era of climate change. *Food Policy* **35**(5), 365–377 (2010).
- 5. Oelkers, E. H., Hering, J. G. & Zhu, C. Water: Is there a global crisis?. Elements 7(3), 157-162 (2011).
- 6. Margerum, R. D. & Robinson, C. J. Collaborative partnerships and the challenges for sustainable water management. Curr. Opin. Environ. Sustain. 12, 53-58 (2015).
- 7. Hoekstra, A. Y. & Chapagain, A. K. Globalization of Water: Sharing the Planet's Freshwater Resources (John Wiley & Sons, 2011).
- 8. https://www.ibef.org/industry/textiles (accessed 8 September 2024).
- 9. Robinson, T., McMullan, G., Marchant, R. & Nigam, P. Remediation of dyes in textile effluent: A critical review on current treatment technologies with a proposed alternative. Bioresour. Technol. 77(3), 247-255 (2001).
- 10. https://oizom.com/most-polluting-industries/ (accessed 8 September 2024).
 11. Hoekstra, A. Y., Chapagain, A. K. & Van Oel, P. R. Advancing water footprint assessment research: Challenges in monitoring progress towards sustainable development goal 6. Water 9(6), 438 (2017).
- 12. Hoekstra, A. Y., Hung, P. Q. Virtual water trade. In Proceedings of the International Expert Meeting on Virtual Water Trade, 2003, 12, 1-244
- 13. Hubbe, M. A., Hasan, S. H. & Ducoste, J. J. Cellulosic substrates for removal of pollutants from aqueous systems: A review. 1. Metals. BioResources 6(2), 2161-2287 (2011).
- 14. Bafana, A., Devi, S. S. & Chakrabarti, T. Azo dyes: Past, present and the future. Environ. Rev. 19, 350-371 (2011).

- 15. Carliell, C. M., Barclay, S. J., Shaw, C., Wheatley, A. D. & Buckley, C. A. The effect of salts used in textile dyeing on microbial decolourization of a reactive azo dye. *Environ. Technol.* 19(11), 1133–1137 (1998).
- Combes, R. D. & Haveland-Smith, R. B. A review of the genotoxicity of food, drug and cosmetic colours and other azo, triphenylmethane and xanthene dyes. Mutat. Res. 98(2), 101–243 (1982).
- 17. Green, F. J. The sigma-aldrich handbook of stains, dyes and indicators. Aldrich Chemical Co, 1990.
- 18. de Lima, R. O. A. et al. Mutagenic and carcinogenic potential of a textile azo dye processing plant effluent that impacts a drinking water source. *Mutat. Res.* **626**(1–2), 53–60 (2007).
- 19. Szyguła, A., Guibal, E., Ruiz, M. & Sastre, A. M. The removal of sulphonated azo-dyes by coagulation with chitosan. *Colloids Surf.* A 330, 219–226 (2008).
- 20. Dávila-Jiménez, M. M., Elizalde-González, M. P. & Peláez- Cid, A. A. Adsorption interaction between natural adsorbents and textile dyes in aqueous solution. *Colloids Surf. A* 254, 107–114 (2005).
- 21. Alkan, M., Demirbas, Ö. & Doğan, M. Adsorption kinetics and thermodynamics of an anionic dye onto sepiolite. *Microporous Mesoporous Mater.* **101**(3), 388–396 (2007).
- 22. Vimonses, V., Lei, S., Jin, B., Chow, C. W. & Saint, C. Adsorption of congo red by three Australian kaolins. *Appl. Clay Sci.* 43(3–4), 465–472 (2009).
- 23. Ghosh, D. & Bhattacharyya, K. G. Adsorption of methylene blue on kaolinite. Appl. Clay Sci. 20(6), 295-300 (2002).
- Bulut, E., Özacar, M. & Şengil, İA. Equilibrium and kinetic data and process design for adsorption of Congo Red onto bentonite. J. Hazard. Mater. 154(1–3), 613–622 (2008).
- Miranda-Trevino, J. C. & Coles, C. A. Kaolinite properties, structure and influence of metal retention on pH. Appl. Clay Sci. 23(1-4), 133-139 (2003).
- 26. Schoonheydt, R. A. & Johnston, C. T. Surface and interface chemistry of clay minerals. Dev. Clay Sci. 1, 87-113 (2006).
- 27. Sheldon, R. A. Organic synthesis-past, present and future. Chem. Ind. 23, 903-906 (1992).
- 28. Pashaei, S., Hosseinzadeh, S. & Syed, A. A. Studies on coconut shell powder and crysnanoclay incorporated acrylonitrile butadiene rubber/styrene butadiene rubber (NBR/SBR) green nanocomposites. *Polym. Compos.* **38**(4), 727–735 (2017).
- 29. Taqui, S. N., Yahya, R., Hassan, A., Nayak, N. & Syed, A. A. A novel sustainable design to develop polypropylene and unsaturated polyester resin polymer composites from waste of major polluting industries and investigation on their physicomechanical and wear properties. *Polym. Compos.* 40(3), 1142–1157 (2019).
- 30. Taqui, S. N., Yahya, R., Hassan, A., Nayak, N. & Syed, A. A. Adsorption of Acid Blue 113 from aqueous solution onto nutraceutical industrial coriander seed spent: Isotherm, kinetics, thermodynamics and modeling studies. *Desalin. Water Treat.* **153**, 321–337 (2019).
- 31. Taqui, S. N. et al. Sustainable adsorption method for the remediation of crystal violet dye using nutraceutical industrial fenugreek seed spent. *Appl. Sci.* 11(16), 7635 (2021).
- 32. Sulthana, R. et al. Adsorption of crystal violet dye from aqueous solution using industrial pepper seed spent: Equilibrium, thermodynamic, and kinetic studies. Adsorpt. Sci. Technol. 2022, 9009214 (2022).
- 33. Taqui, S. N. et al. A practical approach to demonstrate the circular economy in remediation of textile dyes using nutraceutical industrial spent. RSC. Adv. 14(36), 26464–26483 (2024).
- 34. Straub, R., Voyksner, R. D. & Keever, J. T. Thermospray, particle beam and electrospray liquid chromatography-mass spectrometry of azo dyes. *J. Chromatogr. A* 627(1–2), 173–186 (1992).
- 35. Blakemore, W. M. et al. Characterization, purification, and analysis of solvent yellow 33 and solvent green 3 dyes. *J. Chromatogr. A* 391, 219–231 (1987).
- https://www.sigmaaldrich.com/IN/en/product/aldrich/210439?srsltid=AfmBOooh2rUkwddIpsm7SlRmwKCuRirVdHwr8w_PH m0Yy8u2HdsHFoNR (accessed on 15th January 2025).
- 37. Chowdhury, S. & Das, P. Utilization of a domestic waste—Eggshells for removal of hazardous malachite green from aqueous solutions. *Environ. Prog. Sustain.* 31(3), 415–425 (2012).
- 38. Langmuir, I. The constitution and fundamental properties of solids and liquids. Part I. Solids. J. Am. Chem. Soc. 38(11), 2221–2295 (1916).
- 39. Webber, T. W. & Chakravorti, R. K. Pore and solid diffusion models for fixed-bed adsorbers. AIChE J. 20(2), 228-238 (1974).
- 40. Freundlich, H. M. F. Over the adsorption in solution. J. Phys. Chem. 57(385471), 1100-1107 (1906).
- 41. Jovanović, D. S. Physical adsorption of gases. Kolloid Z. Z. Polym. 235(1), 1203-1213 (1969).
- 42. Dubinin, M. M. The equation of the characteristic curve of activated charcoal. In Dokl. Akad. Nauk. SSSR. 1947, 55, 327–329
- 43. Toth, J. State equation of the solid-gas interface layers. Acta Chim. Hung. 69, 311-328 (1971).
- 44. Sips, R. Combined form of Langmuir and Freundlich equations. J. Phys. Chem. 16(429), 490-495 (1948).
- 45. Radke, C. J. & Prausnitz, J. M. Thermodynamics of multi-solute adsorption from dilute liquid solutions. AIChE J. 18(4), 761–768 (1972).
- 46. Redlich, O. & Peterson, D. L. A useful adsorption isotherm. J. Phys. Chem. 63, 1024-1026 (1959).
- 47. Vieth, W. R. & Sladek, K. J. A model for diffusion in a glassy polymer. J. Colloid Sci. 20(9), 1014–1033 (1965).
- 48. Brouers, F., Sotolongo, O., Marquez, F. & Pirard, J. P. Microporous and heterogeneous surface adsorption isotherms arising from Levy distributions. *Phys. A. Stat.* **349**(1–2), 271–282 (2005).
- 49. Lagergren, S. K. About the theory of so-called adsorption of soluble substances. Sven. Vetenskapsakad. Handingarl. 24, 1-39 (1898).
- 50. Ho, Y. S. & McKay, G. Sorption of dye from aqueous solution by peat. Chem. Eng. J. 70(2), 115-124 (1998).
- 51. Wang, H. L., Chen, J. L. & Zhai, Z. C. Study on thermodynamics and kinetics of adsorption of p-toluidine from aqueous solution by hypercrosslinked polymeric adsorbents. *Environ. Chem.* **23**(2), 188–192 (2004).
- Boyd, G. E., Adamson, A. W. & Myers, L. S. Jr. The exchange adsorption of ions from aqueous solutions by organic zeolites. II. Kinetics 1. J. Am. Chem. Soc. 69(11), 2836–2848 (1947).
- 53. Kumar, P., Prasad, B., Mishra, I. M. & Chand, S. Catalytic thermal treatment of desizing wastewaters. *J. Hazard. Mater.* **149**, 26–34 (2007).
- 54. Talarposhti, A. M., Donnelly, T. & Anderson, G. K. Colour removal from a simulated dye wastewater using a two-phase anaerobic packed bed reactor. *Water Res.* 35, 425–432 (2001).
- 55. Standard Methods for the Examination of Water and Wastewater, 20th ed. (American Public Health Association, Washington DC, 2002)
- 56. Balarak, D., Zafariyan, M., Igwegbe, C. A., Onyechi, K. K. & Ighalo, J. O. Adsorption of acid blue 92 dye from aqueous solutions by single-walled carbon nanotubes: Isothermal, kinetic, and thermodynamic studies. *Environ. Process.* 8, 869–888 (2021).
- 57. Balarak, D., Ganji, F., Choi, S. S., Lee, S. M. & Shim, M. J. Effects of operational parameters on the removal of acid blue 25 dye from aqueous solutions by electrocoagulation. *Appl. Chem. Eng.* **30**(6), 742–748 (2019).
- 58. Al-Musawi, T. J., Rajiv, P., Mengelizadeh, N., Mohammed, I. A. & Balarak, D. Development of sonophotocatalytic process for degradation of acid orange 7 dye by using titanium dioxide nanoparticles/graphene oxide nanocomposite as a catalyst. *J. Environ. Manag.* 292, 112777 (2021).
- 59. Gülen, J., Akın, B. & Özgür, M. Ultrasonic-assisted adsorption of methylene blue on sumac leaves. *Desal. Water. Treat.* **57**(20), 9286–9295 (2016).
- 60. Gülen, J. & Deler, Ö. The potential capability of treated perlite for removal of penta chloro nitrobenzene. Z. Phys. Chem. 238(6), 1103–1121 (2024).

- 61. Balarak, D., Abasizadeh, H., Yang, J.-K., Shim, M. J. & Lee, S.-M. Biosorption of Acid Orange 7 (AO7) dye by canola waste: Equilibrium, kinetic and thermodynamics studies. *Desalin. Water Treat.* **190**, 331–339 (2020).
- 62. Balarak, D., Al-Musawi, T. J., Mohammed, I. A. & Abasizadeh, H. The eradication of reactive black 5 dye liquid wastes using *Azolla filiculoides* aquatic fern as a good and an economical biosorption agent. SN Appl. Sci. 2, 1–11 (2020).
- 63. Gülen, J., Altın, Z. & Özgür, M. Removal of amitraz from aqueous solutions on clay by adsorption technique at industrial scale. *Mater. Test.* **59**, 94–100 (2017).
- 64. Gülen, J. & Gezerman, A. O. A novel biosorbent for remediation of colored waste water. *Biomass Convers. Biorefin.* 13, 3227–3235 (2023).
- Gülen, J. & Karpuz, Ö. A concise approach for interpreting the removal kinetic of 2, 4-D by carbonized peanut shell. J. Dispers. Sci. Technol. 1–10 (2024).
- Gülen, J. & Zorbay, F. Methylene blue adsorption on a low cost adsorbent—Carbonized peanut shell. Water Environ. Res. 89, 805–816 (2017).
- 67. Gülen, J. & Aslan, S. Adsorption of 2, 4-dichlorophenoxyacetic acid from aqueous solution using carbonized chest nut as low cost adsorbent: kinetic and thermodynamic. Z. Phys. Chem. 234, 461–484 (2020).
- Gülen, J. & İskeçeli, M. Removal of methylene blue by using porous carbon adsorbent prepared from carbonized chestnut shell. Mater. Test. 59, 188–194 (2017).
- 69. Gülen, J., Küçük, İ, Yalçın, B. S., Çelik, S. E. & Özgür, M. Ultrasonic supported dye removal by a novel biomass. Z. Phys. Chem. 236, 1651–1670 (2022).

Acknowledgement

The authors extend their appreciation to the Deanship of Research and Graduate Studies at King Khalid University for funding this work through Large Research Project under grant number RGP2/67/46.

Author contributions

"M.A.H.D.A.: conceptualization; methodology; investigation; validation; writing—original draft; S.N.T.: conceptualization; methodology; investigation; validation; formal analysis; resources; writing—original draft; writing—review and editing. U.T.S.: conceptualization; methodology; investigation; validation; writing—original draft; writing—review and editing S.A.Y.: conceptualization; methodology; investigation; validation; writing—original draft; writing—review and editing. R.S.: investigation; formal analysis. R.A.M.: investigation; formal analysis, A.A.S.: investigation; formal analysis. S.J.U.: investigation; formal analysis. M.A.: investigation; formal analysis. S.I.: investigation; formal analysis. All authors have read and agreed to the published version of the manuscript".

Declarations

Competing interests

The authors declare no competing interests.

Additional information

Correspondence and requests for materials should be addressed to A.A.S. or W.A.K.

Reprints and permissions information is available at www.nature.com/reprints.

Publisher's note Springer Nature remains neutral with regard to jurisdictional claims in published maps and institutional affiliations.

Open Access This article is licensed under a Creative Commons Attribution-NonCommercial-NoDerivatives 4.0 International License, which permits any non-commercial use, sharing, distribution and reproduction in any medium or format, as long as you give appropriate credit to the original author(s) and the source, provide a link to the Creative Commons licence, and indicate if you modified the licensed material. You do not have permission under this licence to share adapted material derived from this article or parts of it. The images or other third party material in this article are included in the article's Creative Commons licence, unless indicated otherwise in a credit line to the material. If material is not included in the article's Creative Commons licence and your intended use is not permitted by statutory regulation or exceeds the permitted use, you will need to obtain permission directly from the copyright holder. To view a copy of this licence, visit http://creativecommons.org/licenses/by-nc-nd/4.0/.

© The Author(s) 2025